Clays and Clay Minerals, Vol. 48, No. 1, 111–119, 2000.

TRANSMISSION ELECTRON MICROSCOPY OF SYNTHETIC 2- AND 6-LINE FERRIHYDRITE

DAWN E. JANNEY,[1] JOHN M. COWLEY,[2] AND PETER R. BUSECK[1]

[1]Departments of Geology and Chemistry/Biochemistry and
[2]Department of Physics and Astronomy, Arizona State University, Tempe, Arizona 85287, USA

Abstract—High-resolution transmission electron microscopy (HRTEM), selected-area electron diffraction (SAED), annular dark-field scanning transmission electron microscope (STEM) images, and electron nanodiffraction were used to examine structures of synthetic 2- and 6-line ferrihydrite specimens. HRTEM images of 2-line ferrihydrite (2LFh) show scattered small (~1–3 nm) areas with lattice fringes surrounded by areas free of fringes. All SAED patterns show two bright rings corresponding to *d*-values of ~0.15 and 0.25 nm; each ring has a conspicuous shoulder on each side. Faint rings corresponding to *d*-values of 0.08, 0.095, 0.100, 0.106–0.114 (very broad ring), and 0.122 nm are visible in strongly exposed SAED patterns. Nanodiffraction patterns show conspicuous streaks and a lack of superlattice formation.

HRTEM images of 6-line ferrihydrite (6LFh) display larger crystallites (typically ~5–6 nm) with lattice fringes visible in many thin areas. SAED patterns show rings corresponding to *d*-values of 0.148, 0.156, 0.176, 0.202, 0.227, and 0.25–0.26 nm and a shoulder extending between *d*-values of ~0.25 and 0.32 nm. Faint rings corresponding to *d*-values of 0.086, 0.093, 0.107, 0.112, 0.119, 0.125, and 0.135 nm are visible in strongly exposed SAED patterns. Small quantities of hematite, magnetite or maghemite, and an acicular material tentatively identified as goethite were observed in the 6-line ferrihydrite, but these quantities do not contribute significantly to the overall diffracted intensity from the sample.

Key Words—Ferrihydrite, High-Resolution Transmission Electron Microscopy (HRTEM), Nanodiffraction, Selected-Area Electron Diffraction (SAED).

INTRODUCTION

Ferrihydrite is a common iron oxide mineral in low-temperature surface environments such as soils, lake-bottom sediments, drainage ditches, and hot- and cold-spring deposits (*e.g.,* Chukhrov *et al.,* 1973; Schwertmann and Fischer, 1973; Childs *et al.,* 1986; Schwertmann *et al.,* 1987; Schwertmann, 1988; Schwertmann and Taylor, 1989). Because of its small grain size (≤6 nm) and large surface area (hundreds of square meters per gram), even small amounts of ferrihydrite can have important consequences for many soil properties (Cornell and Schwertmann, 1996; Jambor and Dutrizac, 1998; Childs, 1992). Ferrihydrite also occurs as an aqueous alteration product in meteorites (Li *et al.,* 1999; Brearley, 1997; Lee *et al.,* 1996), and it is an important corrosion product of iron and steel. Naturally occurring ferrihydrite can be formed by biological processes (*e.g.,* Chukhrov *et al.,* 1973; Schwertmann and Fischer, 1973; Konhauser, 1997).

Ferrihydrite is important in environmental geology because of its common occurrence in mine-waste environments and its demonstrated ability to adsorb or form coprecipitates with organic compounds and ions of a wide variety of elements (Jambor and Dutrizac, 1998; Alpers *et al.,* 1994; Bigham, 1994; Jambor, 1994). Natural ferrihydrite is difficult to isolate and characteristically contains impurities, even a few mole percent of which may have significant effects on its structure and phase-transition behavior (Parfitt, 1992; Paige *et al.,* 1997; Cornell and Schwertmann, 1996). Thus, most investigations of the chemical and crystallographic characteristics of ferrihydrite use synthetic samples comparable to those in this study.

The number of peaks in X-ray diffraction (XRD) patterns of ferrihydrite is variable. It is common to designate ferrihydrite samples by the number of peaks corresponding to *d*-values from ~0.15 to ~0.25 nm, for example "2-line ferrihydrite (2LFh)," and "6-line ferrihydrite (6LFh)." We follow this convention; however, only synthetic 6LFh samples are strictly consistent with the International Mineralogical Association definition (Fleischer *et al.,* 1975; Farmer, 1992). Other commonly used names for ferrihydrite include "protoferrihydrite" (the name originally proposed for 2LFh), "amorphous ferric oxide," and "hydrous ferric oxide" (*e.g.,* Chukhrov *et al.,* 1973; Towe and Bradley, 1976; Farmer, 1992; Manceau *et al.,* 1995).

Although both natural and synthetic ferrihydrite occur in forms with intermediate numbers of peaks (Carlson and Schwertmann, 1981; Childs *et al.,* 1986; Brearley, 1997; Lee *et al.,* 1996; Lewis and Cardile, 1989; Li *et al.,* 1999; Schwertmann *et al.,* 1999), only synthetic 2LFh and 6LFh have been widely used for structural and chemical studies. Under appropriate conditions, ferrihydrite can transform to hematite, goethite, lepidocrocite, magnetite, or maghemite (Cornell and Schwertmann, 1996; Campbell *et al.,* 1997). To our knowledge, transformations among the forms of ferrihydrite with varying numbers of peaks have not been demonstrated.

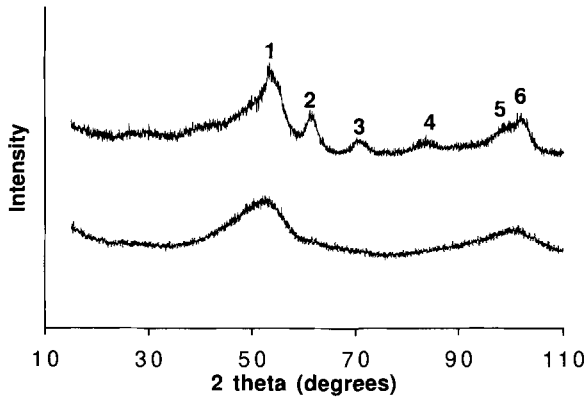

Figure 1. XRD patterns of ferrihydrite: 6LFh (top) and 2LFh (bottom) (CrKα radiation). Numbers above the pattern of 6LFh indicate peaks used in identification.

Despite an early suggestion that 36% of the iron in 6LFh is in tetrahedral coordination (Eggleton and Fitzpatrick, 1988), synchrotron techniques have shown that essentially all of the iron in the interiors of 6LFh crystals is octahedrally coordinated (*e.g.,* Combes *et al.,* 1989, 1990; Manceau and Drits, 1993; Zhao *et al.,* 1993; Shinoda *et al.,* 1994; Waychunas *et al.,* 1996). Intermediate-range structures involving possible corner-, edge-, and face-sharing between octahedra remain subjects of active investigation (Combes *et al.,* 1989, 1990; Waychunas *et al.,* 1993, 1996; Manceau and Drits, 1993; Shinoda *et al.,* 1994) as do coordination environments of iron atoms at crystal surfaces (Zhao *et al.,* 1994; Manceau and Gates, 1997). Longer-range structures (on a scale of a few nm) and the resulting numbers of peaks in XRD patterns were investigated using simulated X-ray diffraction (Drits *et al.,* 1993), leading to the suggestions that ferrihydrite is a mixture containing 25% normal hematite and that the main structural difference between 2LFh and 6LFh may be the size of the coherently diffracting domains (Drits *et al.,* 1993; Manceau and Drits, 1993). However, direct observations to test these suggestions are lacking.

We used high-resolution transmission electron microscopy (HRTEM), selected-area electron diffraction (SAED), dark-field scanning transmission electron microscope (STEM) images, and electron nanodiffraction to study samples of synthetic 2LFh and 6LFh. Our research has two goals: 1) to use direct observations to explore structural similarities and differences between the samples and 2) to provide HRTEM and electron diffraction data on characteristics of synthetic 2LFh and 6LFh because of their importance for chemical and environmental studies.

SAMPLES AND METHODS

Samples of 2LFh and 6LFh were synthesized at the Lehrstuhl für Bodenkunde, Technische Universität München, using methods from Schwertmann and Cornell (1991). The 2LFh was synthesized by adding a 1 M solution of reagent-grade potassium hydroxide to a 0.2 M solution of reagent-grade ferric nitrate with constant stirring until the pH reached 7–8, and repeatedly washing and centrifuging to remove remaining electrolytes. The 6LFh was synthesized by adding 20 g ferric nitrate to 2 L of distilled water that had been preheated to 75°C, holding the solution at 75°C for 10–12 min, cooling it with ice water, and dialyzing to remove electrolytes. The resulting precipitates in both cases were freeze-dried.

Samples were prepared for powder XRD by grinding them gently, moistening them with propanol, spreading them on a zero-background quartz plate, and allowing them to air-dry. XRD patterns (Figure 1) were measured by summing ten scans using CrKα radiation from a Rigaku RU200B diffractometer with a rotating-anode source and a diffracted-beam curved-graphite monochromator. Each scan used a 0.05° step size and a counting time of 0.5 s per step for 6LFh or 1.0 s per step for 2LFh, which diffracted less strongly. The resulting XRD patterns are similar to published patterns for both natural and synthetic 2LFh and 6LFh (*e.g.,* Eggleton and Fitzpatrick, 1988; Schwertmann and Cornell, 1991; Cornell and Schwertmann, 1996; Drits *et al.,* 1993).

TEM samples were prepared by ultrasonicating a small amount of ferrihydrite powder in a few drops of high-purity water for 2–3 h, then placing a droplet of the faintly colored water on a holey-carbon or holey-silicon-monoxide film supported by a copper-mesh TEM grid. A cold-water bath was used during ultrasonication to inhibit the possible formation of more crystalline iron minerals. Ultrasonication did not completely separate individual crystals but produced aggregates with electron-transparent edges.

HRTEM images were obtained using a JEOL 4000EX microscope operating at 400 kV (point-to-point resolution 0.17 nm) and a Topcon 002B microscope operating at 200 kV (point-to-point resolution 0.18 nm). Samples with silicon monoxide substrates were less useful because of electron-beam-induced charging. The best images were obtained from thin edges of ferrihydrite aggregates that were supported by the holey-carbon substrate at several points.

SAED patterns were obtained using the smallest selected-area aperture available on each microscope and a camera length that produced a difference of ~7 mm in radii of rings diffracted from *d*-values of 0.15 and 0.25 nm. At least two films were taken of each diffraction pattern: one or more using relatively short exposures (typically ≤45 s) to show diffraction from *d*-values larger than ~0.25 nm and one long exposure (typically 90–180 s) to emphasize *d*-values smaller than ~0.35 nm. Rings representing *d*-values <0.15 nm

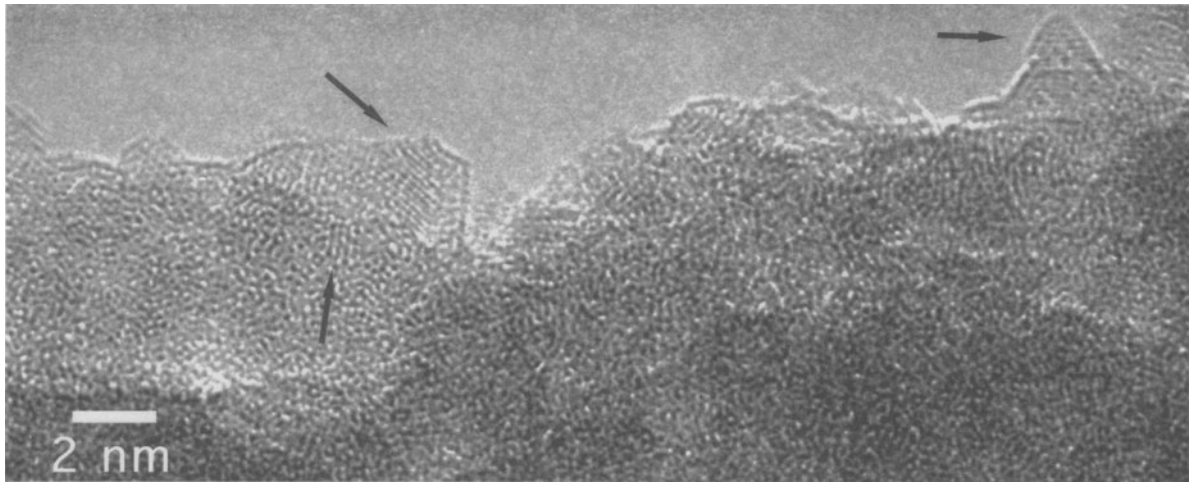

Figure 2. HRTEM image of 2LFh showing single crystallites and material without lattice fringes at edge of aggregate. Note small groups of lattice fringes (examples at arrows), and straight edges of crystallites along thin edges.

were always faint, and could only be measured on the most strongly exposed negatives.

Nanodiffraction patterns (Cowley, 1998) were obtained with a Vacuum Generators HB-5 Scanning Transmission Electron Microscope (STEM) using a beam diameter of ~0.7 nm. Because of the small beam convergence angle and the small thickness of the crystallites, these patterns do not show the same detail inside individual spots as obtained in conventional convergent-beam electron diffraction patterns. Instead, spots in nanodiffraction patterns are interpreted as though they were enlarged reflections in SAED patterns. Despite the small sizes of the crystallites and their tendency to be superposed on each other, zone-axis nanodiffraction patterns in which only one crystallite was strongly diffracting could be obtained. Annular-dark-field STEM images (Cowley, 1998), which are formed using electrons diffracted by the specimen into a ring-shaped region of reciprocal space corresponding to *d*-values of ~0.1–0.3 nm, were obtained to show sizes and shapes of coherently diffracting domains.

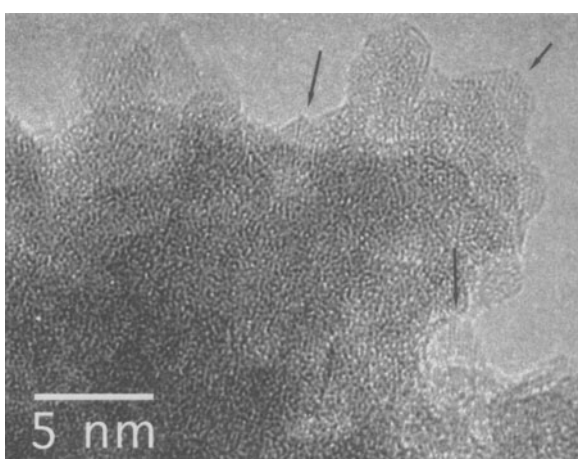

Figure 3. HRTEM image of 2LFh showing possibly hexagonal crystallites. Arrows indicate examples of areas with lattice fringes.

RESULTS

Characteristics of 2LFh

Figures 2 and 3 show HRTEM images of the edges of 2LFh aggregates. Most crystallites are 2–4 nm across and approximately equant. With rare exceptions, each crystallite shows only a single orientation of lattice fringes. Many crystallites display straight edges meeting at angles of ~110°–150° (as measured in images). Although these geometries do not suffice to identify morphologies uniquely, they are consistent with an approximately hexagonal shape. Lattice fringes commonly either parallel the edges of the crystals or bisect the intersection angles.

Widely scattered areas that have distinct lattice fringes are surrounded by areas without recognizable fringes. Although nanodiffraction shows that the sample contains some near-amorphous material, areas without lattice fringes in HRTEM images can also be produced by crystallites that are not in appropriate orientations or are superposed on each other.

All SAED patterns of 2LFh appear similar, suggesting a high degree of homogeneity in the sample (Figure 4; Table 1). Each pattern has two bright rings, each of which has a shoulder on each side. SAED patterns of the holey-carbon substrate by itself have broad, diffuse rings whose centers are at ~0.215 and ~0.12 nm, which overlap the 2LFh pattern. The silicon-monoxide substrate also produces two rings that do not overlap those of the ferrihydrite but are too faint to measure in SAED patterns obtained under the

https://doi.org/10.1346/CCMN.2000.0480114 Published online by Cambridge University Press

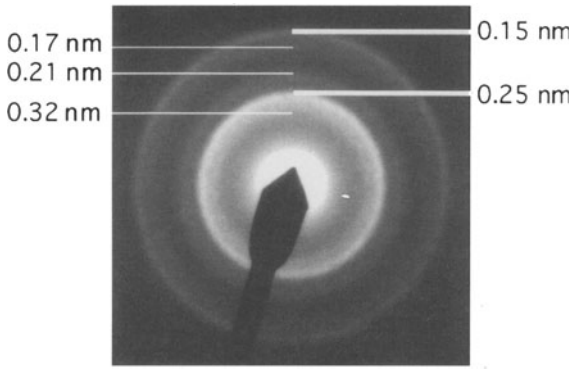

Figure 4. SAED pattern of 2LFh with *d*-values of rings (thick lines) and edges of shoulders (thin lines).

conditions used for ferrihydrite; however, this substrate was not used for most observations because of difficulties with sample charging. 2LFh rings and shoulders can be distinguished from holey-carbon rings by their sharp edges in SAED patterns, as confirmed by comparison of SAED patterns from samples prepared with holey-carbon and silicon-monoxide substrates. The 2LFh shoulder at 0.21–0.25 nm is much brighter than the 0.215-nm holey-carbon ring in SAED patterns from areas including significant quantities of ferrihydrite.

Several nanodiffraction patterns display streaks suggesting a high degree of disorder in the stacking of lattice planes (Figure 5). The absence of distinct reflections along the streaks indicates a lack of longer-range superlattice organization.

Characteristics of 6LFh

Figures 6 and 7 show representative images of 6LFh. Images of thin areas observed at approximately Scherzer defocus display parallel dark and bright lines or alternating black and white spots. These are interpreted as structure images, in which dark and light areas correspond, respectively, to areas of high and low electron density in the crystal structures projected onto a plane perpendicular to the electron beam. Details of images depend on crystallographic orientation relative to the beam; thus, the same structure may appear to be different when seen from different orientations.

Most crystallites are 5–6 nm across, although individuals ranging in size from ~2 to ~11 nm were observed. Most crystallites are equant, with rounded shapes or with straight edges meeting at large angles, suggesting a spherical or polyhedral habit. Reflections from individual crystallites are clearly visible in SAED patterns of 6LFh. These reflections may appear as scattered individuals or closely spaced along rings (Figure 8; Table 2).

Widely scattered larger crystals with tabular or acicular shapes are embedded in the 6LFh. Lattice-fringe

Table 1. Diffraction characteristics of 2LFh.

d-values (nm) from SAED	*d*-values (nm) from XRD (Figure 1)	Description	References
0.32		Edge of intense shoulder extending to 0.25-nm ring	
0.25	0.256	Intense ring	1, 2
0.21		Edge of shoulder extending to 0.25-nm ring	
0.17		Edge of shoulder extending to 0.15-nm ring	
0.15	0.148	Intense ring	1, 2
0.13		Edge of shoulder extending to 0.15-nm ring	
0.122		Ring	
0.106–0.114		Very broad ring	
0.100		Ring	
0.095		Ring	
0.08		Broad ring	

References: 1) Eggleton and Fitzpatrick, 1988 (synthetic); 2) Drits *et al.*, 1993 (synthetic).

geometries do not allow a unique identification. The habits of the acicular crystals are consistent with goethite, which is a likely byproduct of the synthesis method used for 6LFh (Schwertmann and Cornell, 1991).

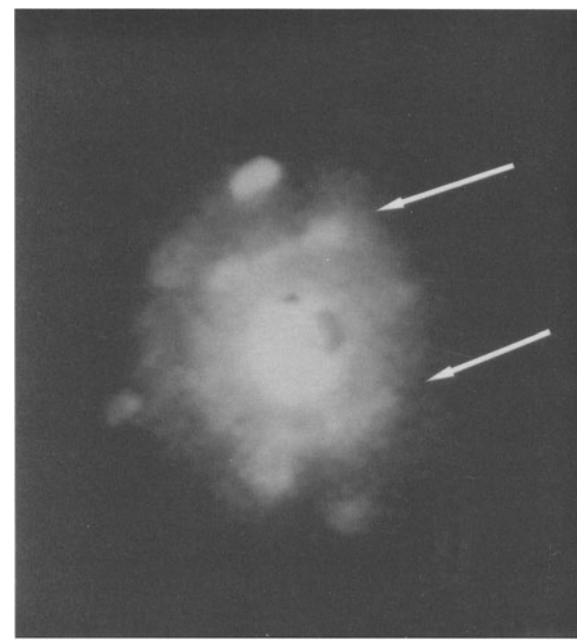

Figure 5. Nanodiffraction pattern of 2LFh with arrows indicating streaks. Diffuse scattering around the center of the pattern is from amorphous carbon deposited as a contaminant on the specimen during analysis.

https://doi.org/10.1346/CCMN.2000.0480114 Published online by Cambridge University Press

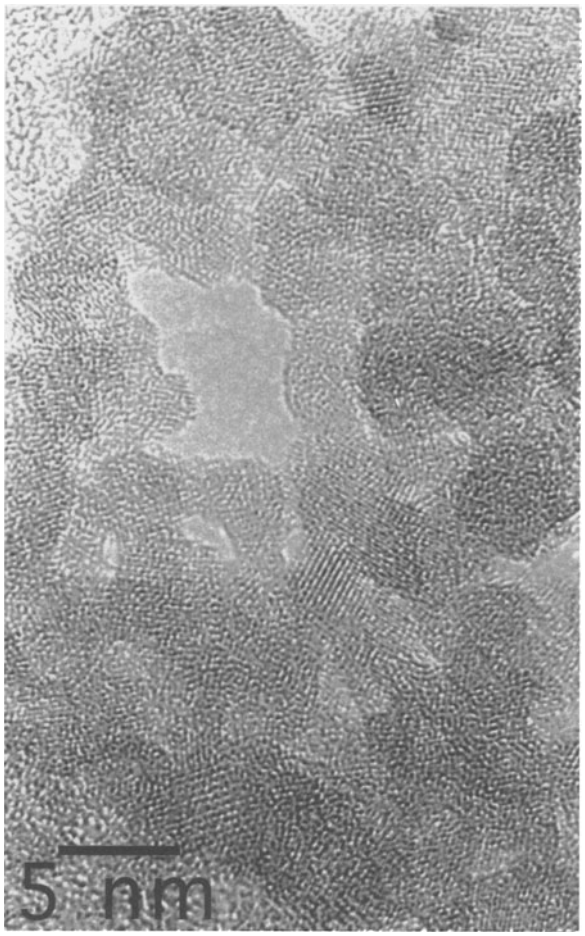

Figure 6. HRTEM image of 6LFh. Note homogeneous grain sizes, rounded-to-hexagonal shapes, variation in lattice-fringe spacing, and high degree of crystallinity as indicated by the large fraction of grains showing lattice fringes or alignment of black and white spots. Material under the scale bar is the holey-carbon substrate.

A few SAED patterns show widely scattered faint reflections corresponding to *d*-values of 0.186 and 0.366 nm, which may represent diffraction from the (024) and (012) planes of hematite (*d*-values 0.184 and 0.368 nm). These reflections, whose diffracted intensities are, respectively, 40 and 30% of that of the highest-intensity hematite reflection in powder samples (ICDD card 33-664), are the most intense hematite reflections that do not superpose any of the 6LFh rings or the 0.25–0.32 nm shoulder. Other SAED patterns (*e.g.,* Figure 8) have individual reflections with *d*-values of 0.275 nm, which may represent diffraction from the (104) plane of hematite (*d*-value 0.270 nm, relative intensity 100%). Estimates of the numbers of hematite and 6LFh crystallites represented in the SAED patterns (obtained by counting individual reflections with *d*-values of ~0.27 and 0.37 for hematite and by dividing the area of the sample incorporated in each SAED pattern by the cross-sectional area of a single 5-nm crystallite for 6LFh) suggest that the ratio of hematite to ferrihydrite crystallites is on the order of 0.1–1%. Although it is likely that other hematite crystals are present in orientations that do not produce distinctive reflections, hematite is clearly not a major constituent of 6LFh.

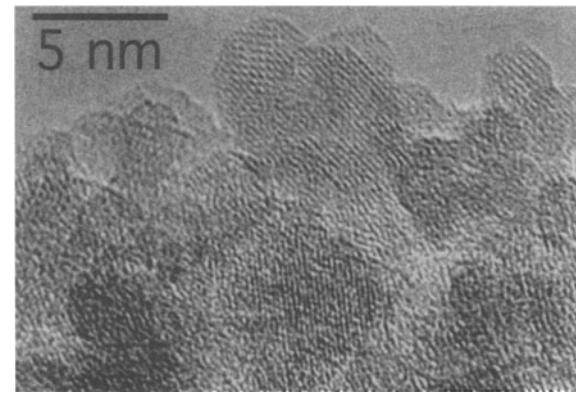

Figure 7. HRTEM image of 6LFh showing details of lattice-fringe geometries.

A small number of SAED patterns from thick particles that did not disaggregate well during ultrasonication show *d*-values of 0.147, 0.160, 0.209, 0.250, 0.29–0.31, and 0.48 nm, which are consistent with magnetite or maghemite (Cornell and Schwertmann, 1996). These SAED patterns do not show recognizable 6LFh rings, suggesting that the magnetite or maghemite occurs in isolated parts of the specimen rather than being dispersed like the hematite and goethite.

Many nanodiffraction patterns of 6LFh show reflections that superpose to form streaks (Figure 9). If these reflections are interpreted as resulting from widely spaced parallel planes, they represent a superlattice; however, singly or multiply twinned crystals may produce a similar effect. The nanodiffraction patterns also suggest that the 6LFh sample contains a small amount

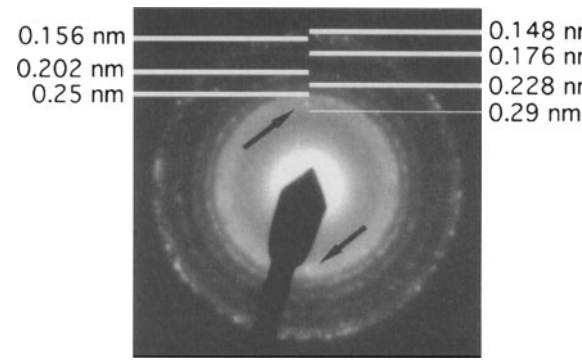

Figure 8. SAED pattern of 6LFh with *d*-values of rings (thick lines) and edge of shoulder (thin line). Sharp reflections indicated by arrows, which have a 0.275-nm *d*-value, are probably from one hematite crystal.

https://doi.org/10.1346/CCMN.2000.0480114 Published online by Cambridge University Press

Table 2. Diffraction characteristics of 6LFh.

d-values (nm) from SAED	*d*-values (nm) from XRD (Figure 1)	Description	References
	0.456	Not observed	
0.366		Rare individual reflections [hematite (012)?]	
0.30–0.32	0.321	Edge of intense shoulder extending to 0.25-nm ring	1, 2, 3
0.275		Rare individual reflections [hematite (104)?]	4
0.25–0.26	0.252	Intense ring	1, 2, 3, 4, 5, 6
0.227	0.222	Ring	1, 2, 3, 5, 6
0.202	0.196	Ring	1, 2, 3, 4, 5, 6
0.186		Rare, faint individual reflections [hematite (024)?]	
0.176	0.170	Ring	1, 2, 3, 4, 5, 6
0.145–0.158	0.147, 0.149	Broad zone containing large numbers of individual reflections; many SAEDs contain distinct rings at 0.148 and 0.156 nm	1, 2, 3, 4, 5, 6
0.135		Ring	
0.125		Ring (visible in only one SAED)	
0.119		Ring	
0.112		Ring	
0.107		Broad, relatively intense ring	
0.093		Ring	
0.086		Relatively intense ring	

References: 1) Eggleton and Fitzpatrick, 1988 (synthetic); 2) Drits *et al.*, 1993 (synthetic); 3) Towe and Bradley, 1976 (synthetic); 4) Childs *et al.*, 1986 (natural); 5) Carlson and Schwertmann, 1981 (natural); 6) Van der Giessen, 1966 (synthetic).

of near-amorphous material. Annular dark-field images show rounded, coherently diffracting domains 3–10 nm across (Figure 10); in at least one case, a coherently diffracting domain occupies only part of a rounded particle similar to those interpreted as single crystallites in HRTEM images. Nanodiffraction patterns from different parts of this domain show significant variations in the degree of streaking, suggesting differences in the extent of disorder within the domain. Fringes in annular dark-field images with periods of 1, 1.6, or 2.7 nm may represent Moiré fringes from overlapping crystallites.

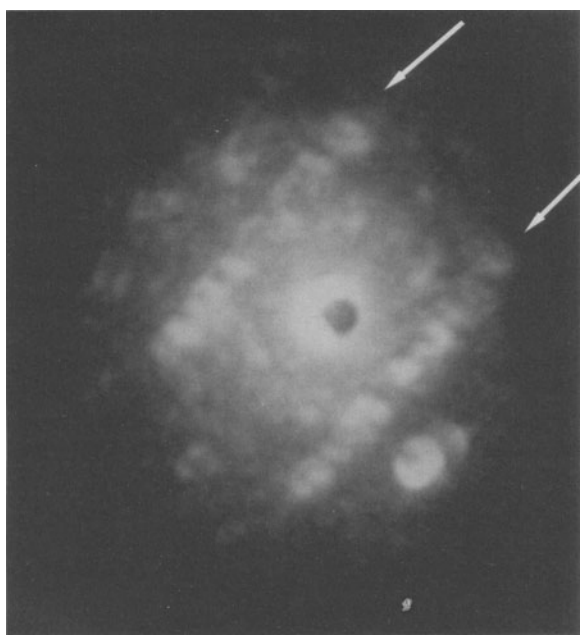

Figure 9. Nanodiffraction pattern of 6LFh. Arrows indicate streaks consisting of overlapping individual reflections.

DISCUSSION

Our results corroborate previous HRTEM observations of synthetic 2LFh and 6LFh (Eggleton and Fitzpatrick, 1988) in several respects. The 2LFh and 6LFh

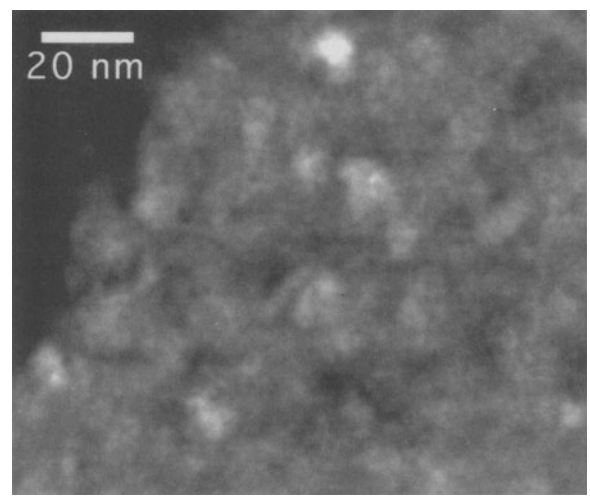

Figure 10. STEM dark-field image of 6LFh showing shapes and sizes of coherently diffracting domains. Brightness in image depends on orientation of the crystal relative to the beam; brightest areas are diffracting most strongly.

https://doi.org/10.1346/CCMN.2000.0480114 Published online by Cambridge University Press

samples both consist of aggregates of individual crystallites that can be at least partially disaggregated by ultrasonication; the 6LFh disaggregates more readily than the 2LFh. Crystals with well-developed hexagonal outlines are common in 6LFh and are less abundant in 2LFh. Neither the 2LFh nor the 6LFh is sensitive to the electron beam, even when exposed to the high electron density of the HB-5 STEM. Annular dark-field images and closely spaced reflections in 6LFh nanodiffraction patterns are consistent with the existence of a superlattice, which may have the previously reported 0.94-nm spacing (Eggleton and Fitzpatrick, 1988).

Our results differ significantly from HRTEM observations of natural 2LFh and 6LFh (Eggleton, 1987). The natural specimens are reportedly amorphous and consist of aggregates of spheres 5–10 nm across, many of which have electron-dense margins 0.2–0.3 nm thick. These characteristics suggest that the natural ferrihydrite formed as a series of spherical bubbles, perhaps followed by crystallization within the bubble walls. This formation process is unlike that of synthetic 2LFh, which forms by hydrolysis and increasing polymerization of iron octahedra (Combes *et al.,* 1989). Differences between the natural samples and our synthetic samples probably reflect some combination of the structural consequences of the incorporation of small quantities of Si into natural ferrihydrites (*e.g.,* Parfitt *et al.,* 1992) and different formation processes.

Although several *d*-values obtained from SAED patterns are slightly larger than the corresponding values from our XRD patterns, all differences are less than ~0.01 nm (Tables 1 and 2). Our data are also consistent with previously published *d*-values between 0.15–0.25 nm for both natural and synthetic ferrihydrite (Carlson and Schwertmann, 1981; Childs *et al.,* 1986; Chukhrov *et al.,* 1973; Drits *et al.,* 1993; Eggleton and Fitzpatrick, 1988; Towe and Bradley, 1976; Van der Giessen, 1966).

The edges of the shoulders in SAED patterns of 2LFh do not correspond to recognizable features in our XRD patterns of 2LFh but have approximately the same *d*-values as peaks in 6LFh (Tables 1 and 2); they also correspond to small changes in slope in the XRD pattern of 2LFh collected by Drits *et al.* (1993). The sharpness and consistency of the radii of the shoulder edges measured in SAED patterns from different crystals indicate that the shoulders are consequences of structural variations in 2LFh rather than artifacts introduced by electron diffraction. At least three phenomena may contribute to these variations: fine-scale mixtures containing several kinds of crystallites or a combination of crystallites and amorphous material; small structural differences between the interiors of crystallites and their surfaces, which are estimated to involve 30–50% of the atoms in a spherical 2-nm crystal (Manceau and Gates, 1997; Combes *et al.,* 1989; Zhao *et al.,* 1994); and structural variations in the interiors of individual crystallites (Combes *et al.,* 1989). Variations in nanodiffraction patterns taken within a single diffracting domain in the 6LFh are difficult to explain purely in terms of mixtures or of surface characteristics.

It has been proposed that the main structural difference between 2LFh and 6LFh is the size of their coherently diffracting domains and that both are mixtures containing ~25% hematite (Drits *et al.,* 1993; Manceau and Drits, 1993). Our data do not support these ideas: the relative absence of lattice fringes in 2LFh images, the smaller number of rings in 2LFh SAED patterns, and the absence of distinct reflections in the streaks in nanodiffraction patterns all suggest that the crystal structure of 2LFh is less developed than that of the 6LFh. Further studies using nanodiffraction are being undertaken to clarify these differences.

With the possible exception of one small crystal that could not be identified, hematite was not found in any 2LFh image; there are also no reflections that can be uniquely attributed to hematite in any 2LFh diffraction pattern. Although a small quantity of hematite is present in the 6LFh sample, there are two reasons why it probably does not account for the high-diffracted intensity from *d*-values from 0.26 to 0.27 nm, as assumed in the model of Drits *et al.* (1993): a) the quantity of hematite is too small; and b) the presumed hematite reflections are relatively sharp, whereas the shoulder is a region of slowly varying intensity in which individual reflections can only rarely be identified.

In summary, our data confirm reported differences in particle sizes between 2LFh and 6LFh and indicate that there are significant structural differences. The 2LFh is homogeneous and does not contain significant quantities of crystalline impurities. HRTEM images of 2LFh show at most one orientation of lattice fringes in each crystallite, consistent with previous suggestions that it may have only two-dimensional order. In contrast, 6LFh is slightly less homogeneous: HRTEM images and SAED patterns show small quantities of other crystalline substances, and there is some variability in SAED patterns. The 6LFh has a well-developed structure and may have some superlattice development.

ACKNOWLEDGMENTS

We thank U. Schwertmann for providing the samples and for numerous helpful discussions. We also acknowledge the Center for High Resolution Electron Microscopy at ASU for microscope access (and training for DEJ), and T. Groy for assistance in collecting XRD data. Reviews by P. Heaney and J. Post resulted in significant improvements to the manuscript. Funding was provided by NSF grant EAR9706359.

REFERENCES

Alpers, C.N., Blowes, D.W., Nordstrom, D.K., and Jambor, J.M. (1994) Secondary minerals and acid mine-water

chemistry. In *The Environmental Geochemistry of Sulfide Mine-Wastes,* D.W. Blowes and J.L. Jambor, eds., Mineralogical Association of Canada, Nepean, Ontario, 247–270.

Bigham, J.M. (1994) Mineralogy of ochre deposits formed by sulfide oxidation. In *The Environmental Geochemistry of Sulfide Mine-Wastes,* D.W. Blowes and J.L. Jambor, eds., Mineralogical Association of Canada, Nepean, Ontario, 103–132.

Brearley, A.J. (1997) Phyllosilicates in the matrix of the unique carbonaceous chondrite Lewis Cliff 85332 and possible implications for the aqueous alteration of CI chondrites. *Meteoritics and Planetary Science,* **32,** 377–388.

Campbell, A.S., Schwertmann, U., and Campbell, P.A. (1997), Formation of cubic phases on heating ferrihydrite. *Clay Minerals,* **32,** 615–622.

Carlson, L. and Schwertmann, U. (1981) Natural ferrihydrites in surface deposits from Finland and their association with silica. *Geochimica et Cosmochimica Acta,* **45,** 421–429.

Childs, C.W. (1992) Ferrihydrite: A review of structure, properties and occurrence in relation to soils. *Zeitschrift für Pflanzenernährung und Bodenkunde,* **155,** 441–448.

Childs, C.W., Wells, N., and Downes, C.J. (1986) Kokowai Springs, Mount Egmont, New Zealand: Chemistry and mineralogy of the ochre (ferrihydrite) deposit and analysis of the waters. *Journal of the Royal Society of New Zealand,* **16,** 85–99.

Chukhrov, F.V., Zvyagin, B.B., Gorshkov, A.I., Yermilova, L.P., and Balashova, V.V. (1973) O Ferrigidrite. [Trans. Fleischer, M. (1974)] *International Geology Review,* **16,** 1131–1143.

Combes, J.M., Manceau, A., Calas, G., and Bottero, J.Y. (1989) Formation of ferric oxides from aqueous solutions: A polyhedral approach by X-ray absorption spectroscopy: I. Hydrolysis and formation of ferric gels. *Geochimica et Cosmochimica Acta,* **53,** 583–594.

Combes, J.M., Manceau, A., and Calas, G. (1990) Formation of ferric oxides from aqueous solutions: A polyhedral approach by X-ray absorption spectroscopy: II. Hematite formation from ferric gels. *Geochimica et Cosmochimica Acta,* **54,** 1083–1091.

Cornell, R.M. and Schwertmann, U. (1996) *The Iron Oxides: Structure, Properties, Reactions, Occurrence and Uses.* VCH, Weinheim, Germany, 573 pp.

Cowley, J.M. (1998) Electron nanodiffraction and STEM imaging of nanoparticles and nanotubes. In *Cluster Materials, Advances in Metal and Semiconductor Clusters 4,* M.A. Duncan, ed., JAI Press, Stamford, Connecticut, 67–113.

Drits, V.A., Sakharov, B.A., Salyn, A.L., and Manceau, A. (1993) Structural model for ferrihydrite. *Clay Minerals,* **28,** 185–207.

Eggleton, R.A. (1987) Noncrystalline Fe-Si-Al-oxyhydroxides. *Clays and Clay Minerals,* **35,** 29–37.

Eggleton, R.A. and Fitzpatrick, R.W. (1988) New data and a revised structural model for ferrihydrite. *Clays and Clay Minerals,* **36,** 111–124.

Farmer, V.C. (1992) Possible confusion between so-called ferrihydrites and hisingerites. *Clay Minerals,* **27,** 373–378.

Fleischer, M., Chao, G.Y., and Kato, A. (1975) New mineral names. *American Mineralogist,* **60,** 485–489.

Jambor, J.L. (1994) Mineralogy of sulfide-rich tailings and their oxidation products, In *The Environmental Geochemistry of Sulfide Mine-Wastes,* D.W. Blowes and J.L. Jambor, eds., Mineralogical Association of Canada, Nepean, Ontario, 59–102.

Jambor, J.L. and Dutrizac, J.E. (1998) Occurrence and constitution of natural and synthetic ferrihydrite, a widespread iron oxyhydroxide. *Chemical Reviews,* **98,** 2549–2585.

Konhauser, K.O. (1997) Bacterial iron biomineralization in nature. *FEMS Microbiology Reviews,* **20,** 315–326.

Lee, M.R., Hutchison, R., and Graham, A.L. (1996) Aqueous alteration in the matrix of the Vigarano (CV3) carbonaceous chondrite. *Meteoritics and Planetary Science,* **31,** 477–483.

Lewis, D.G. and Cardile, C.M. (1989) Hydrolysis of Fe^{III} solution to hydrous iron oxides. *Australian Journal of Soil Research,* **27,** 103–115.

Li, J., Hua, X., Janney, D.E., and Buseck, P.R. (1999) Mineralogy of a fine-grained rim in LEW90500 by transmission electron microscopy. *Abstract #1271, Lunar and Planetary Science Conference XXX.*

Manceau, A. and Drits, V.A. (1993) Local structure of ferrihydrite and feroxyhite by EXAFS spectroscopy. *Clay Minerals,* **28,** 165–184.

Manceau, A. and Gates, W.P. (1997) Surface structural model for ferrihydrite. *Clays and Clay Minerals,* **45,** 448–460.

Manceau, A., Ildefonse, Ph., Hazemann, J.-L., Flank, A.-M., and Gallup, D. (1995) Crystal chemistry of hydrous iron silicate scale deposits at the Salton Sea Geothermal Field. *Clays and Clay Minerals,* **43,** 304–317.

Paige, C.R., Snodgrass, W.J., Nicholson, R.V., Scharer, J.M., and He, Q.H. (1997) The effect of phosphate on the transformation of ferrihydrite into crystalline products in alkaline media. *Water, Air, and Soil Pollution,* **97,** 397–412.

Parfitt, R.L., Van der Gaast, S.J., and Childs, C.W. (1992) A structural model for natural siliceous ferrihydrite. *Clays and Clay Minerals,* **40,** 675–681.

Schwertmann, U. (1988) Occurrence and formation of iron oxides in various pedoenvironments. In *Iron in Soils and Clay Minerals,* J.W. Stucki, B.A. Goodman, and U. Schwertmann, eds., NATO ASI (Advanced Science Institute) Series C217, D. Reidel, Dordrecht, Holland, 267–308.

Schwertmann, U. and Cornell, R.M. (1991) *Iron Oxides in the Laboratory.* VCH, Weinheim, Germany, 137 pp.

Schwertmann, U. and Fischer, W.R. (1973) Natural "amorphous" ferric hydroxide. *Geoderma,* **10,** 237–247.

Schwertmann, U. and Taylor, R.M. (1989) Iron Oxides. In *Minerals in Soil Environments, 2nd edition.* J.B. Dixon and S.B. Weed, eds., Soil Science Society of America, Madison, Wisconsin, 379–438.

Schwertmann, U., Carlson, L., and Murad, E. (1987) Properties of iron oxides in two Finnish lakes in relation to the environment of their formation. *Clays and Clay Minerals,* **35,** 297–304.

Schwertmann, U., Friedl, J., and Stanjek, H. (1999) From Fe(III) ions to ferrihydrite and then to hematite. *Journal of Colloid and Interface Science,* **209,** 215–223.

Shinoda, K., Matsubara, E., Muramatsu, A., and Waseda, Y. (1994) Local structure of ferric hydroxide $Fe(OH)_3$ in aqueous solution by the anomalous X-ray scattering and EXAFS methods. *Materials Transactions, JIM,* **35,** 394–398.

Towe, K.M. and Bradley, W.F. (1967) Mineral constitution of colloidal "hydrous ferric oxides." *Journal of Colloid and Interface Science,* **24,** 384–392.

Van der Giessen, A.A. (1966) The structure of iron (III) oxide-hydrate gels. *Journal of Inorganic and Nuclear Chemistry,* **28,** 2155–2159.

Waychunas, G.A., Rea, B.A., Fuller, C.C., and Davis, J.A. (1993) Surface chemistry of ferrihydrite: Part I. EXAFS studies of the geometry of coprecipitated and adsorbed arsenate. *Geochimica et Cosmochimica Acta,* **57,** 2251–2269.

Waychunas, G.A., Fuller, C.C., Rea, B.A., and Davis, J.A. (1996) Wide-angle X-ray scattering (WAXS) study of "two-line" ferrihydrite structure: Effect of arsenate sorption and counterion variation and comparison with

EXAFS results. *Geochimica et Cosmochimica Acta,* **60,** 1765–1781.

Zhao, J., Huggins, F.E., Feng, Z., Lu, F., Shah, N., and Huffman, G.P. (1993) Structure of a nanophase iron oxide catalyst. *Journal of Catalysis,* **143,** 499–509.

Zhao, J., Huggins, F.E., Feng, Z., and Huffman, G.P. (1994) Ferrihydrite: Surface structure and its effects on phase transformation. *Clays and Clay Minerals,* **42,** 737–746.

E-mail of corresponding author: pbuseck@asu.edu

(Received 1 April 1999; accepted 14 August 1999; Ms. 329; A.E. Peter J. Heaney)